ADVANCED MATERIALS

Supporting Information

for *Adv. Mater.*, DOI: 10.1002/adma.201601425

In Situ Nanoscale Electric Field Control of Magnetism by Nanoionics

*Xiaojian Zhu, Jiantao Zhou, Lin Chen, Shanshan Guo, Gang Liu, Run-Wei Li, and Wei D. Lu**

Submitted to ADVANCED MATERIALS

Supporting Information

In-situ Nanoscale Electric Field Control of Magnetism by Nanoionics

*Xiaojian Zhu, Jiantao Zhou, Lin Chen, Shanshan Guo, Gang Liu, Run-Wei Li, and Wei D. Lu**

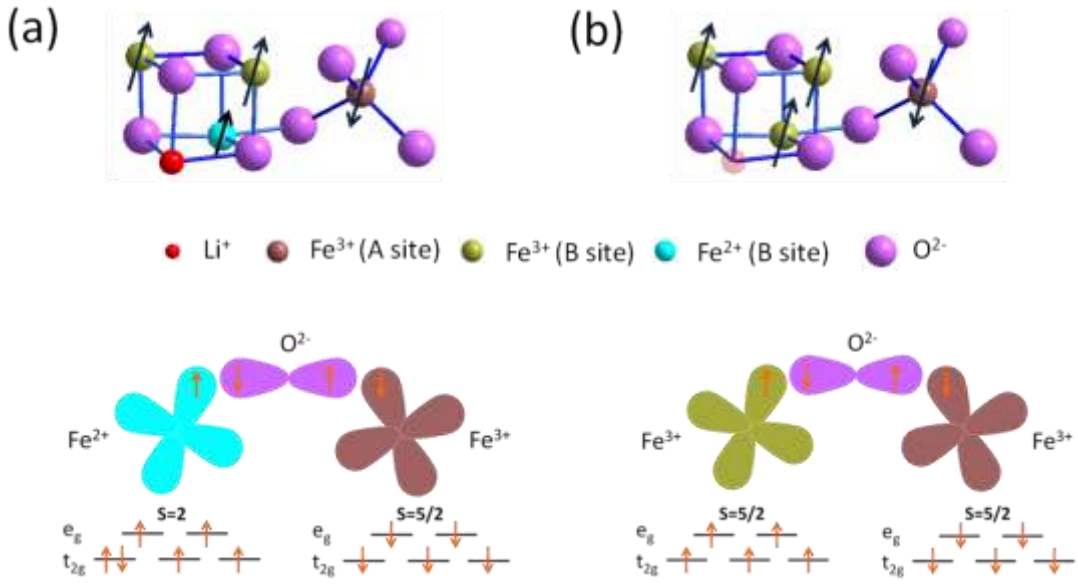

Figure S1. Schematics of the localized lattice structures and electron-orbital interactions showing the magnetic superexchange coupling in LFO (a) before and (b) after the de-intercalation of a Li^+ ion. The de-intercalation process leads to the oxidization of the Fe^{2+} ion (S=2) to an Fe^{3+} ion (S=5/2).

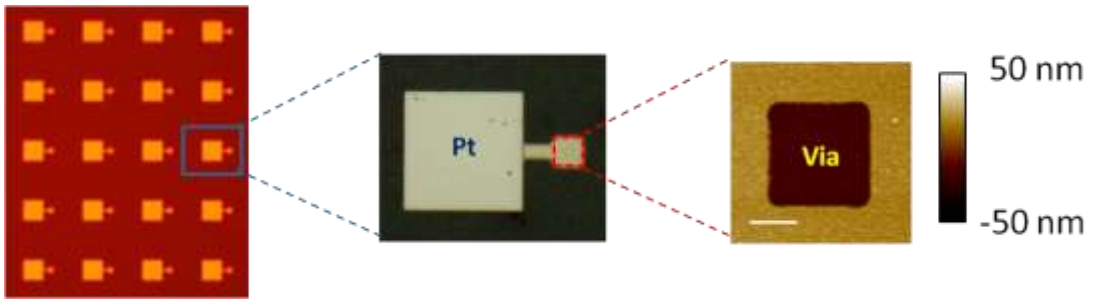

Figure S2. Optical image of the device array (left), an individual device (middle) and corresponding AFM image showing the via-structure. Scale bar: 1 μm.

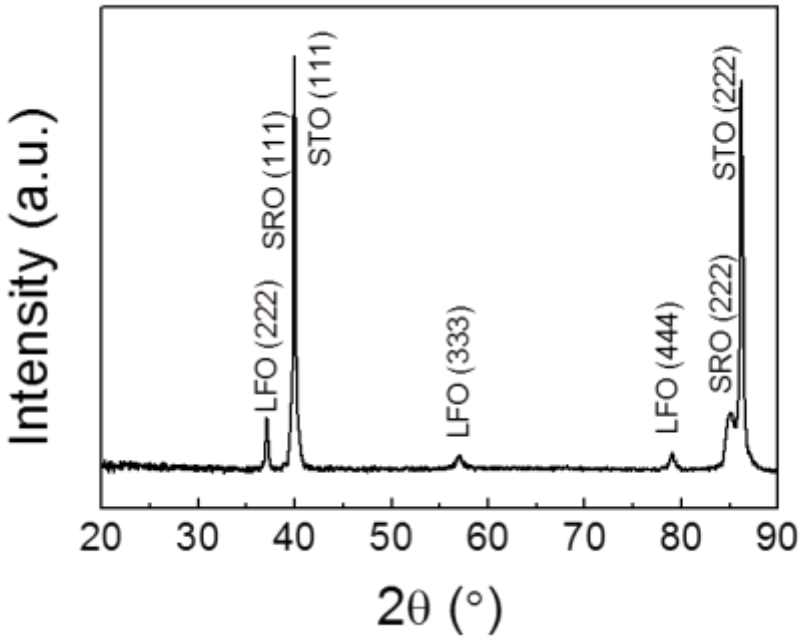

Figure S3. XRD results of the as fabricated LFO/SRO/STO structure.

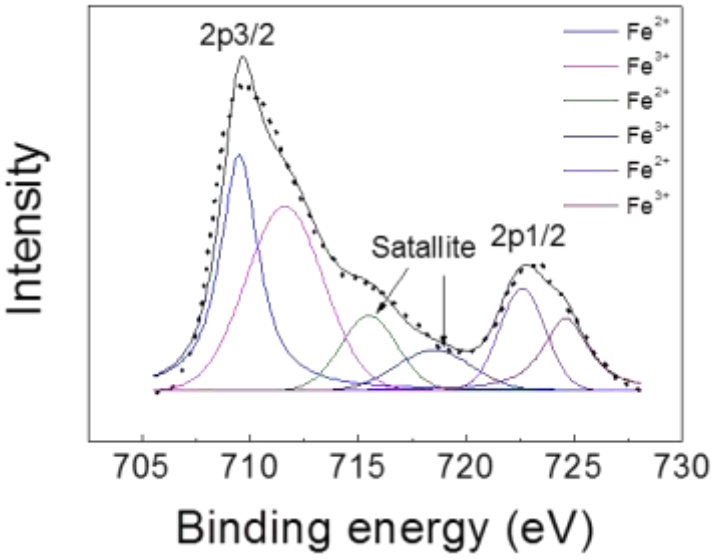

Figure S4. XPS results of the Fe 2p spectra in the as-deposited LFO film showing the existence of Fe^{2+} and Fe^{3+} ions in the film.

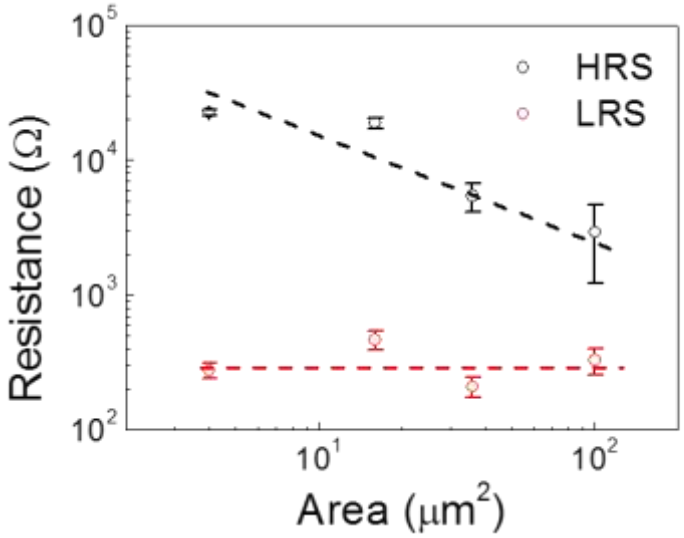

Figure S5. Dependence of the device resistance at HRS and LRS on the electrode area.

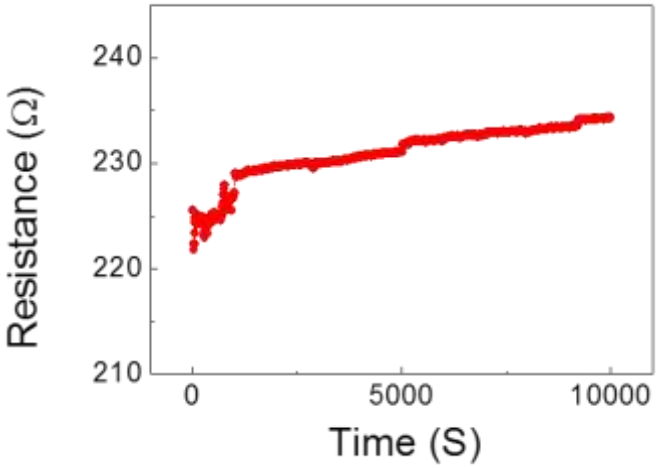

Figure S6. Retention of the device at LRS measured at 100 ℃ (read under 0.2 V).

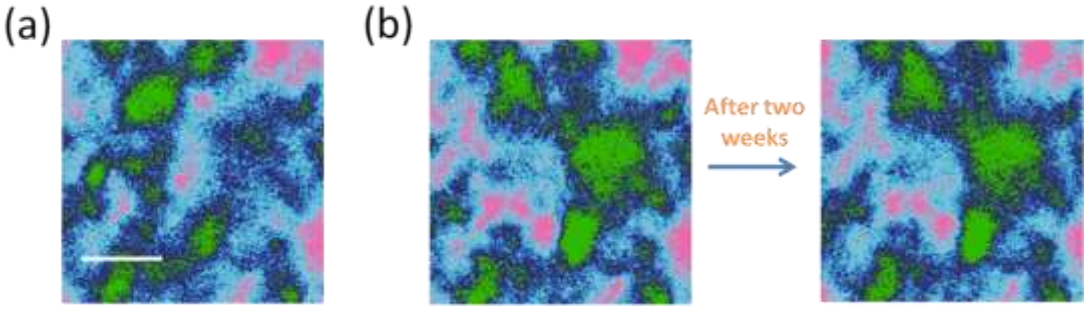

Figure S7. MFM images of a Pt/LFO/SRO device at (a) the VS and (b) the LRS. The modulated magnetic domains were stable without obvious changes after two weeks. Scale bar: 500 nm.

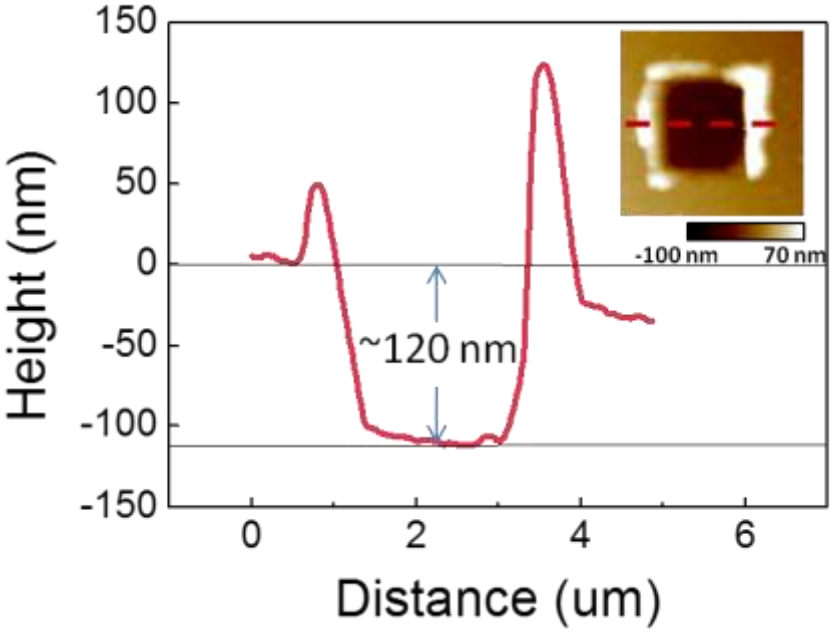

Figure S8. Height profile along the dashed line (inset) in the via region after removing the Pt layer inside the via. The inset is an AFM image showing the morphology of the device after removing the Pt layer inside the via. The initial depth of the via was 60 nm. After removing the Pt layer, the depth was increased to 120 nm, suggesting the complete removal of the 60 nm-thick Pt layer covering the underlying LFO film. The drastic height changes near the edges of the via were attributed to the deformation of the remaining Pt film near the edges.

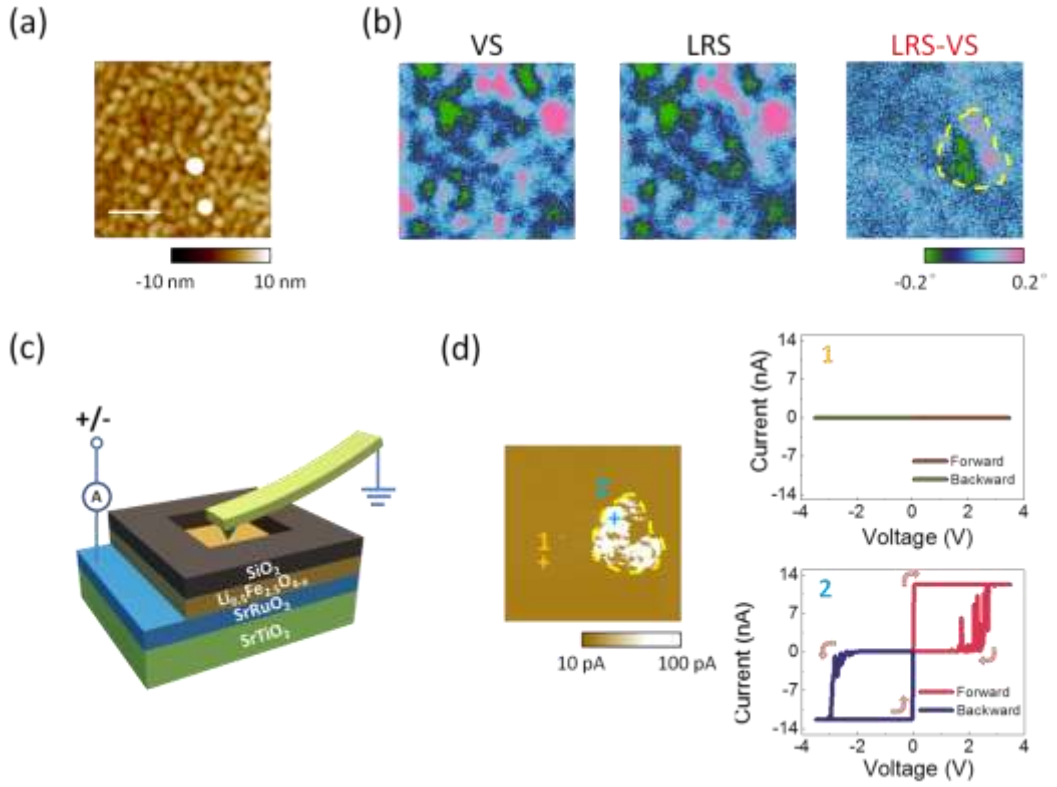

Figure S9. (a) AFM image showing the morphology of a Pt/LFO/SRO device and (b) corresponding MFM images of the device at the VS and the LRS states, and a plot showing the difference between them highlighting the apparent magnetization changes (marked by the dashed region). Scale bar: 500 nm. (c) Schematic of the setup for the CAFM measurement. The conductive tip was grounded and the bias voltage was applied on the SRO electrode. (d) Current map of the device at the LRS at 0.5 V bias, and corresponding *I-V* characteristics measured at positions 1 and 2 as marked in the current map, showing RS behavior in region 2 which also exhibited enhanced conductance compared to the rest of the device area (e.g. region 1).

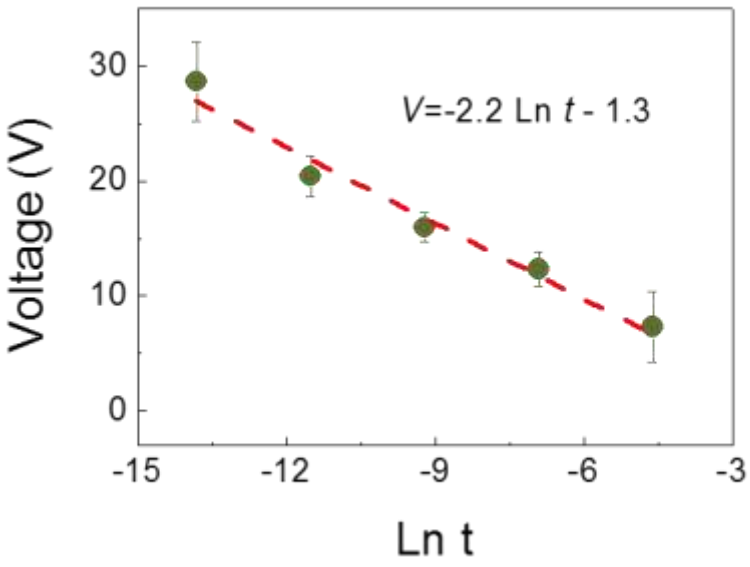

Figure S10 Dependence of the required Forming voltage on the pulse width in Pt/LFO/SRO devices during the Forming process.

Extraction of the ion hopping distance and the hopping energy barrier

According to the ion hopping model,[1,2] the hopping rate *v* of Li^+ ions in the LFO film is dependent on the hopping energy barrier, temperature and the applied electric field, through the relationship

$$v = 2 \cdot a \cdot f \cdot \exp\left(\frac{-qU_a}{kT}\right) \cdot \sinh\left(\frac{qVa}{2kTL}\right), \quad (1)$$

where *a* is the ion hopping distance, f the hoping attempt frequency, q is the charge of an electron, U_a is the activation energy barrier, k is Boltzmann's constant, T is the temperature, V is the applied bias voltage and L is the film thickness. Considering *v* as the average velocity of ion migration during the forming process, *v*=L/t, where L and t corresponded to the film thickness and the width of the pulse required to switch the device to a LRS, and for applied electric field that is high enough (*i.e.* qVa/2kTL>>1), equation (1) can be simplified into

$$\frac{L}{t} = a \cdot f \cdot \exp\left(\frac{-qU_a}{kT}\right) \cdot \exp\left(\frac{qVa}{2kTL}\right), \quad (2)$$

Therefore, the slope and intercept of the V-Ln t curve can be expressed as

$$\text{slope} = \frac{dV}{dLnt} = -\frac{2kTL}{qa}, \quad (3)$$

$$\text{intercept} = Ln\frac{L}{a \cdot f} + \frac{qU_a}{kT} \quad (4).$$

Taking kT (T=300 K)=0.026 eV, L=25 nm and $f=10^{12}$, based on the results shown in Fig. S8, the Li^+ ion hopping distance *a* and the diffusion energy barrier U_a can be extracted to be 0.57 nm and 0.59 eV respectively.

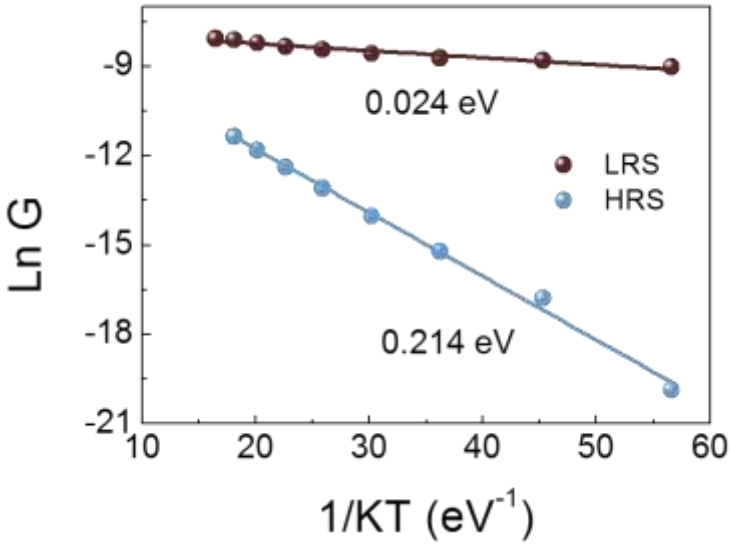

Figure S11. Dependence of the conductance on 1/KT for the Pt/LFO/SRO device at HRS and LRS, showing a thermal-activation behavior in both states.

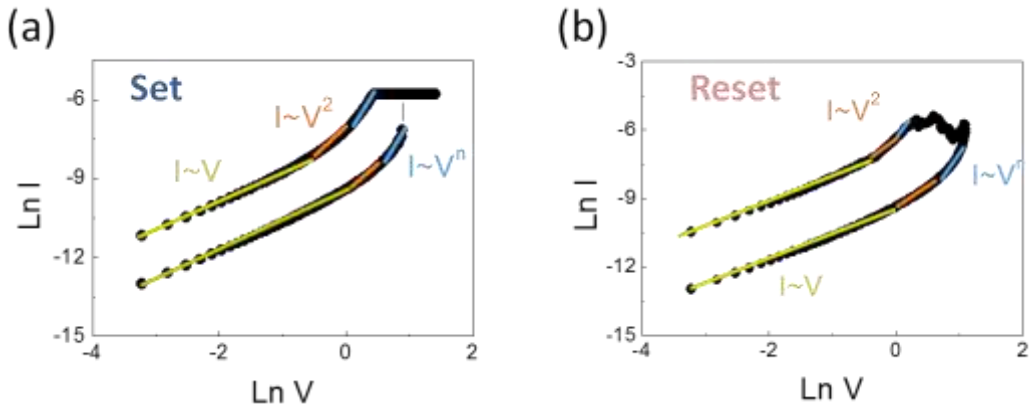

Figure S12. Ln I-Ln V characteristics of the Pt/LFO/SRO device during (a) SET and (b) RESET process and corresponding fitting results using the SCLC model.[3]

Relationship of the phase value in MFM measurements and the sample's magnetization intensity

The magnetic field $\vec{H}(r)$ produced by a magnetic sample can be written as

$$\vec{H}(r) = \sum_J [\frac{3\vec{r_J}(\vec{m_J}\cdot\vec{r_J})}{|\vec{r_J}|^5} - \frac{\vec{m_J}}{|\vec{r_J}|^3}], \quad (5)$$

where $\vec{r_J}$ is the position vector pointing from an elementary magnetic moment in the sample to the position, and $\vec{m_J}$ represents the magnetic moment vector of the elementary magnetic moment.

The magnetic probe in the magnetic field produced by the magnetic sample senses a magnetic force $\vec{F}$, which can be described as

$$\vec{F} = \int_{V_c} \nabla_r(\vec{M_T}(r_v) \cdot \vec{H}(\vec{r} + \vec{r_v}))dV, \quad (6)$$

where $\vec{M_T}(r_v)$ is the magnetic moment vector of an unit volume in the probe, $\vec{H}(\vec{r} + \vec{r_v})$ is the magnetic field vector produced by the magnetic sample, $\vec{r}$ is the vector corresponding to the probe position, $\vec{r_v}$ is the vector corresponding to the elementary magnetic moment position of the probe relative to r, and V_c is the volume of the magnetic layer on the probe.

The phase value ($\Delta\emptyset$) obtained in the MFM image is proportional to the gradient of the interaction force between the magnetic probe and the magnetic stray field produced by the magnetic sample, $\Delta\emptyset = \frac{Q}{k}\frac{\partial F}{\partial z}$, where Q is the vibrating system quality factor, k is the cantilever spring constant, F is the magnetic interaction force and z is the axis perpendicular to the film surface. If we take the magnetic probe as a magnetic dipole with the magnetization direction perpendicular to the sample surface, and only consider the magnetic stray field generated by the magnetic moment of the sample below the magnetic probe, (5) and (6) can be simplified as $H(r) = \frac{2}{d^3}m_S$ and $F(r) = \frac{-6m_P}{d^4}m_S$, where m_p and m_S correspond to the effective magnetic moment dipole of the magnetic probe and the magnetic moment of the sample, respectively, and d corresponds to the distance between the sample and the probe. Thus, the phase value in the MFM image can be simplified as $\Delta\emptyset = \frac{Q}{k}\frac{24m_P}{d^5}m_S$. It can be seen that the measured phase value is proportional to the magnetic moment of the sample.

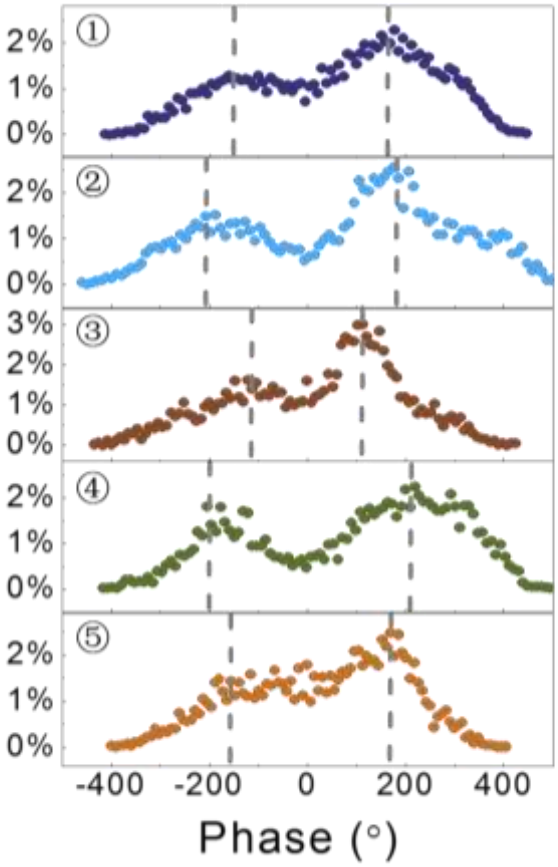

Figure S13. Histograms showing the statistical distribution of the phase values shown in Figure 3c in the main text. The peak positions marked by the dashed lines correspond to the most populated phase values in the upward and downward domains in Figure 3c, respectively. As can be seen here, the most populated phase values shift towards higher (lower) values for both the upward and downward domains after the device was switched to the LRS (HRS), suggesting the increase (decrease) of the overall magnetization during RS.

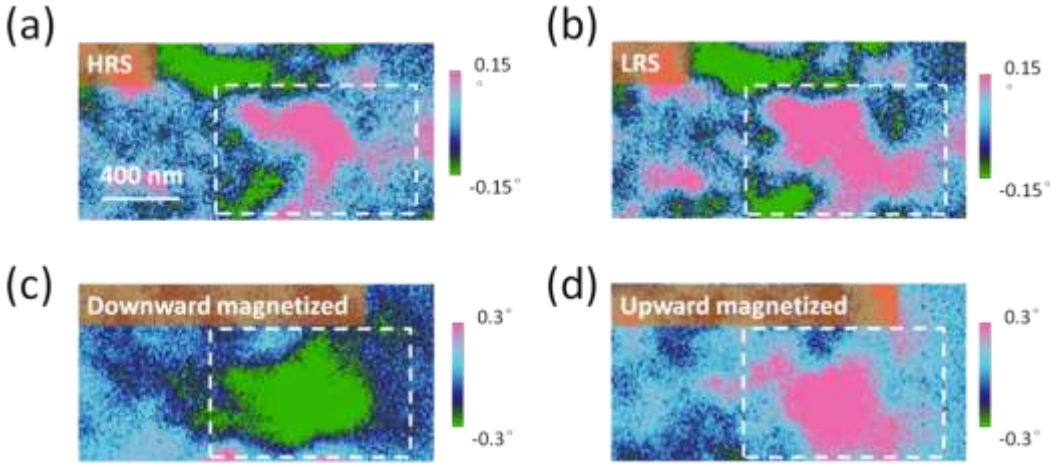

Figure S14. MFM images of a Pt/LFO/SRO device at the (a) HRS, (b) LRS, and after the application of (c) a downward and (d) an upward magnetic field (~2000 Oe) for the LRS case in (b). The downward/upward external magnetic field can switch the magnetic domains to the downward/upward magnetization direction correspondingly.

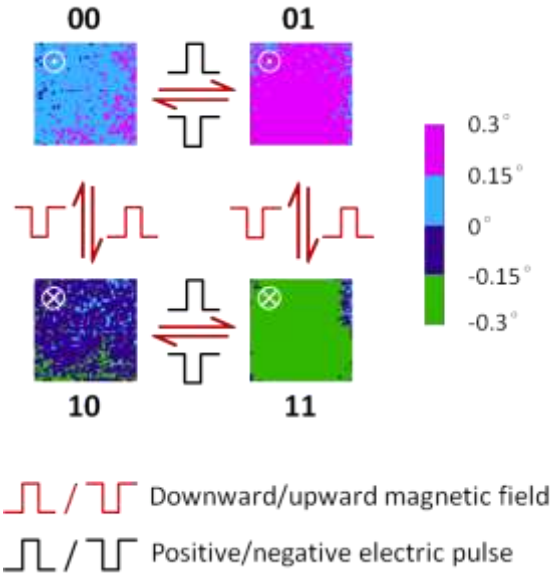

Figure S15. Schematics of a magnetic domain (~200 nm×200 nm) with controlled magnetization direction and intensity for 2-level data storage. The upward (downward) magnetization direction is used to store the first digit of "0" ("1"), and the low (high) magnetization is used to store the second digit of "0" ("1"), respectively. Here, the low and high magnetization is defined as when the overall phase value $|\emptyset|<0.15°$ and $|\emptyset|\geq 0.15°$ respectively. Storage of a new data can be achieved by reversibly controlling the magnetization direction and device resistance (which in turn controls the magnetization) through an external magnetic field (~2000 Oe) and an electric pulse, respectively .

[1] Waser, R., Dittmann, R., Staikov, G., Szot, K. *Adv. Mater.* **2009,** *21,* 2632-2663.

[2] Kim, S., Choi, S., Lu, W. *ACS Nano* **2014,** *8,* 2369-2376.

[3] Xia, Y., He, W., Chen, L., Meng, X., Liu, Z. *Appl. Phys. Lett.* **2007,** *90,* 022907.